

Double-Pair Double-Difference Relocation Improves Depth Precision and Highlights Detailed 3D Fault Geometry for Induced Seismicity in Alberta, Canada

Katherine M. Biegel^{*1}, Jan Dettmer¹, Nadine Igonin², and David W. Eaton¹

Abstract

Precise earthquake locations with well-constrained uncertainties can improve our understanding of faulting. Double-difference relocation methods, particularly event-pair double-difference relocations, are well established and have been applied to large earthquake catalogs to provide fault geometries. Previous adaptations of the event-pair double-difference method include data space extensions to use additional information from station pairs, referred to as double-pair double-difference relocation. We apply double-pair double-difference relocation to data from a dense network of borehole geophones for induced seismicity monitoring. This experiment was acquired in an area with strong lithological variation and sharp velocity contrasts, and most previous studies using this dataset are subject to poorly constrained focal depths. We compare the double-pair double-difference to event-pair double-difference relocations and study the effectiveness and uncertainties of both methods. Although double-pair double-difference relocation does not improve absolute locations, substantially improved relative locations and reduced uncertainties are obtained. The method reduces the impact of path effects in the source region, which is essential for applications where reservoir units in the source region can exhibit strong velocity contrasts, anisotropy, and fractures. From the improved relocation, we produce a detailed 3D fault interpretation of the dataset that constrains the geological interpretation. The improved catalog shows excellent depth constraints with seismicity that is restricted to specific geological units. We interpret that seismicity activated pre-existing faults in the reservoir layer and adjacent units. Notably, the results show no evidence of induced seismicity activating basement structures.

Introduction

Estimating hypocentral parameters (Geiger, 1910) is a fundamental problem in seismology. High-precision earthquake hypocenters, particularly for catalogs with large numbers of events, are essential for detecting and studying faults, temporal and spatial characteristics of seismicity, volcanic activity, and other applications. Even for well-understood and monitored sites, the location uncertainty is often larger than the source dimensions, limiting interpretations.

Many earthquake location methods solve for absolute hypocentral locations. These methods apply either linear approximations (Geiger, 1910; Pavlis, 1986; Shearer, 1997) or nonlinear methods (Billings, 1994; Lomax *et al.*, 2000, 2009; Sambridge and Kennett, 2001). Although linear and nonlinear hypocentral estimation methods employ different methods, they share similar practical and physical issues. For example, both methods depend on knowledge of local velocity

structures. This dependence can be reduced by applying relative location methods.

Relocation methods produce high-precision relative hypocenter locations within event clouds. Although these methods do not improve the absolute location accuracy for individual events, paired events and grouped event geometry are more precisely determined based on travel-time differences. Early relative location studies focused on waveform cross-correlation methods (Poupinet *et al.*, 1984; Deichmann and Garcia-Fernandez, 1992; Dodge *et al.*, 1995). These methods rely on several possible

1. Department of Earth, Energy, and Environment, University of Calgary, Calgary, Alberta, Canada, <https://orcid.org/0000-0001-8682-6169> (KMB); <https://orcid.org/0000-0001-8906-8156> (JD); <https://orcid.org/0000-0001-6495-6093> (DWE); 2. Department of Geoscience, University of Texas at Dallas, Dallas, Texas, U.S.A.

*Corresponding author: katherine.biegel@ucalgary.ca

© Seismological Society of America

event-pairing strategies. Parent-event approaches relate smaller child events to a single, well-determined event location (Ito, 1985; Scherbaum and Wendler, 1986; VanDecar and Crosson, 1990; Lees, 1998). Similarly, joint-hypocenter methods determine the relative locations of similar event doublets (Fréchet, 1985) based on the shared or averaged hypocenter of earthquake pairs (Jordan and Sverdrup, 1981; Got *et al.*, 1994; Rodi, 2006). Relative location methods can minimize the effects of velocity structure errors using pairs of events (Pavlis, 1992). However, these methods still depend on the velocity model choices used in the inversion (Michelini and Lomax, 2004). Because of the similar ray paths for event pairs, relative methods can reduce the effects of receiver-region velocity model inaccuracies on event locations by estimating time differences of similar rays.

One of the most commonly applied relative double-difference location methods is event-pair double-difference relocation (Waldhauser and Ellsworth, 2000; hereafter, event-pair relocation). This technique minimizes differential travel times (DTs) that are obtained for event pairs from waveform cross correlations and catalog differential times. This method has been widely applied in studies of natural seismicity (Schaff *et al.*, 2002; Waldhauser *et al.*, 2004; Waldhauser and Schaff, 2008) and induced seismicity (Castellanos and Van der Baan, 2013). Based on reciprocity, station-pair double-difference relocation (hereafter station-pair relocation) has been applied to nonvolcanic tremors (Zhang *et al.*, 2010). This method can improve the event locations of large data sets and pairs data by exploiting similar ray geometries between a single event and pairs of stations.

Guo and Zhang (2017) combined station and event pairs in the double-pair double-difference, sometimes referred to as triple-difference, relocation method (hereafter double-pair relocation). Double-pair relocation relies on similarities in ray geometries in the vicinity of the sources and near the stations. Double-pair relocation has been applied in regional-scale seismicity studies (Guo and Zhang, 2017; Li *et al.*, 2018; Ogwari *et al.*, 2018; Share *et al.*, 2021) and geothermal microseismicity studies for small numbers of events and stations (Guo *et al.*, 2023). It has been proposed that double-pair relocations can improve absolute and relative location errors in areas with velocity heterogeneities in both the source and receiver regions if station coverage is sufficiently dense (Guo and Zhang, 2017).

Microseismic data from hydraulic fracturing (HF) monitoring with dense networks provide opportunities for studying relocation methods. Because of the dense station coverage, more events and smaller events can be detected and located using this type of acquisition. Event-pair relocations have been applied to such data (Castellanos and Van der Baan, 2013; Tian *et al.*, 2016; Chen *et al.*, 2017; Dando *et al.*, 2021) and produced sharper seismicity images. However, the analysis of fault architecture and fracture networks is limited by model uncertainties. In unconventional reservoirs, large velocity contrasts in the source region can cause issues for location methods.

Dense networks combined with double-pair relocations have the potential to overcome these limitations.

We apply double-pair relocation to dense network data (Fig. 1a) collected as part of a microseismic monitoring program, the Tony Creek Dual Microseismic Experiment (ToC2ME; Eaton *et al.*, 2018) in Alberta, Canada (Fig. 1b). Data were recorded on 68 borehole geophone stations in an area of 7×7 km. During treatment, over 3500 induced earthquakes were recorded with high signal-to-noise ratios (SNRs). We study the locations and uncertainties of these induced earthquakes (Fig. 2a) and interpret the results in terms of fault architecture. The results show clearly delineated event locations accompanied by reduced uncertainties. The improved locations are interpreted in terms of fault activation and limit-induced events to the injection layer and recover a plausible 3D fault geometry.

Theory and Methods

The event-pair relocation method (Waldhauser and Ellsworth, 2000) solves a linearized inverse problem for location updates for event pairs, events i and j , within a cloud of events with their catalog locations considered as the starting model. Event pairs are defined by proximity for catalog pairs or waveform similarity for cross-correlation pairs. The method is based on the following relationship:

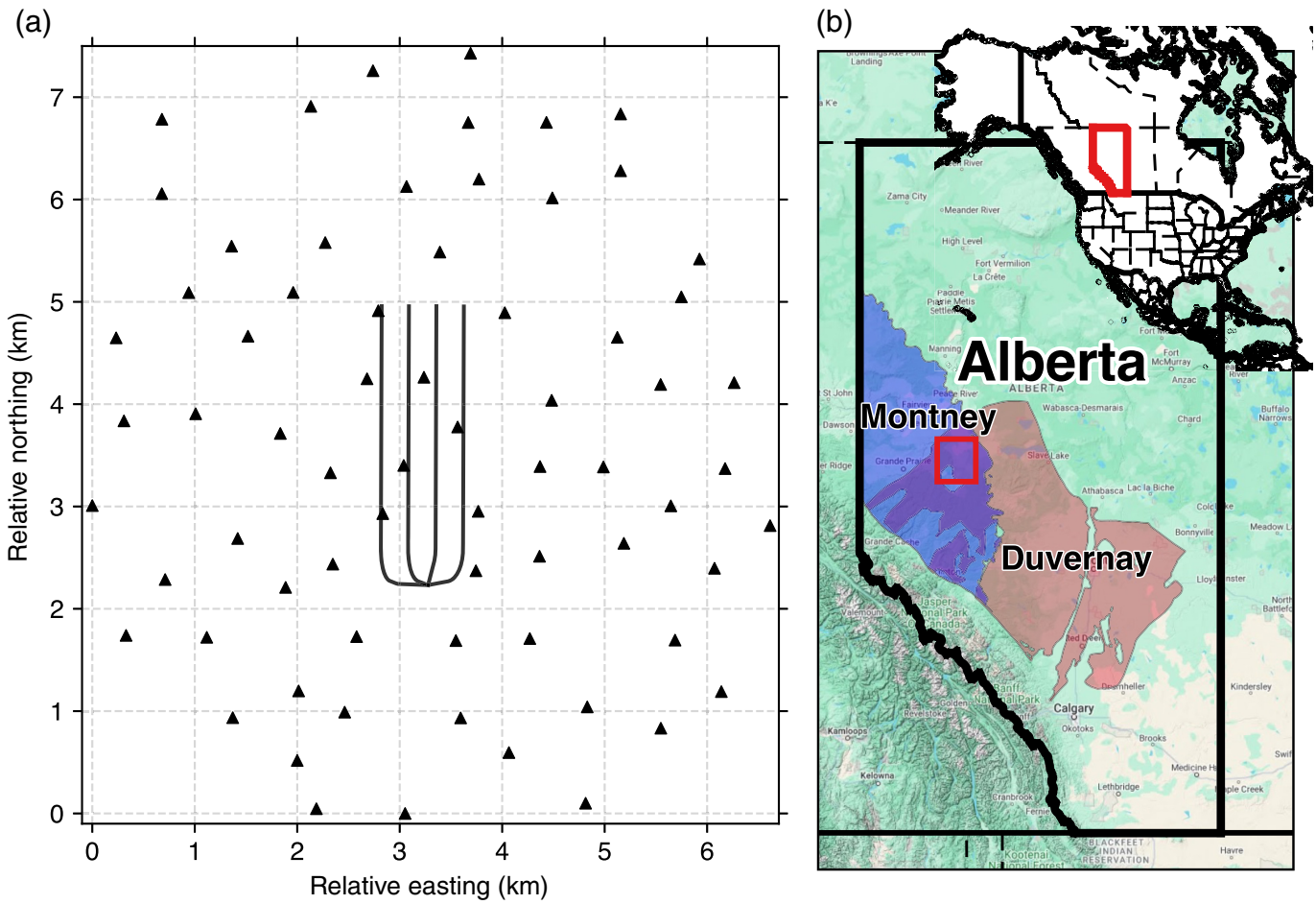
$$\left(\frac{\partial t_k^i}{\partial \mathbf{m}} \Delta \mathbf{m}^i + \Delta \tau_i \right) - \left(\frac{\partial t_k^j}{\partial \mathbf{m}} \Delta \mathbf{m}^j + \Delta \tau_j \right) = dr_k^{ij}, \quad (1)$$

in which dr_k^{ij} are the DT residuals or double differences $(t_k^i - t_k^j)^{\text{obs}} - (t_k^i - t_k^j)^{\text{cal}}$, in which t are the travel times for different event and station configurations. Furthermore, the two vectors of spatial model perturbations $\Delta \mathbf{m}^i$ and $\Delta \mathbf{m}^j$ represent location updates for the event pair whereas the terms $\Delta \tau_i$ and $\Delta \tau_j$ refer to origin time perturbations for the event pairs.

The reciprocal pairing geometry of equation (1) is station-pair double-difference relocation (Zhang *et al.*, 2010). Previous studies (Wolfe, 2002; Zhang *et al.*, 2010; Guo and Zhang, 2017) have noted limitations of using station pairs for relocation due to station separation. Station-pair relocation may exhibit poor sensitivity to some location parameters, particularly depth, if the difference in the partial depth derivatives for the location parameters is small. This situation occurs for raytracing when event-station separations are similar (Wolfe, 2002; Zhang *et al.*, 2010).

Double-pair relocation includes both pair geometries, which removes both source- and station-side effects (Guo and Zhang, 2017). That approach solves for location updates based on double-pair residuals for events i and j at stations k and l according to

$$\left(\frac{\partial t_k^i}{\partial \mathbf{m}} - \frac{\partial t_l^i}{\partial \mathbf{m}} \right) \Delta \mathbf{m}^i + \left(\frac{\partial t_k^j}{\partial \mathbf{m}} - \frac{\partial t_l^j}{\partial \mathbf{m}} \right) \Delta \mathbf{m}^j = dr_{kl}^{ij}, \quad (2)$$



in which the dr_{kl}^{ij} can be solved for by subtracting either pairs of event-pair residuals or station-pair residuals,

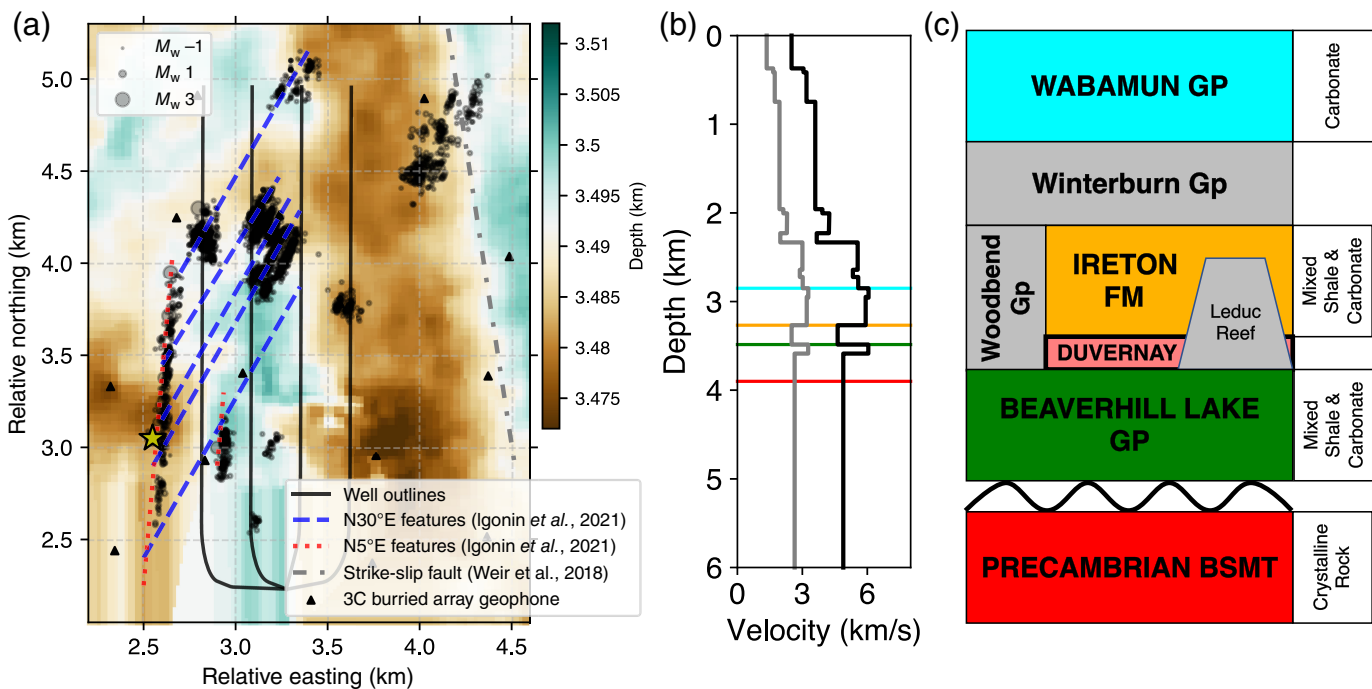
$$\begin{aligned} dr_{kl}^{ij} &= \left\{ \left(t_k^i - t_k^j \right) - \left(t_l^i - t_l^j \right) \right\}^{\text{obs}} - \left\{ \left(t_k^i - t_k^j \right) - \left(t_l^i - t_l^j \right) \right\}^{\text{cal}} \\ &= \left\{ \left(t_k^i - t_l^i \right) - \left(t_k^j - t_l^j \right) \right\}^{\text{obs}} - \left\{ \left(t_k^i - t_l^i \right) - \left(t_k^j - t_l^j \right) \right\}^{\text{cal}}. \end{aligned} \quad (3)$$

Compared to the event- or station-pair relocations, the double-pair relocation only solves for changes to the spatial hypocentral parameters and is less sensitive to the assumed velocity model (Guo and Zhang, 2017). The removal of the origin time term and the station correction term could partially contribute to the improvement in locations seen in double-pair relocation relative to the event- and station-pair methods. The double-pair method does not limit the maximum station-pair separation because the effects of the larger velocity uncertainties can be reduced by the event-pair information.

We apply relocDD-py—an open-source relocation software in Python (Biegel and Dettmer, 2024) based on the hypoDD software (Waldhauser and Ellsworth, 2000) and extended to include station and double pairs. The software solves equations (1) and (2) for model perturbations by inverse conjugate

Figure 1. (a) Tony Creek Dual Microseismic Experiment (ToC2ME) buried geophone network (triangles) centered around the horizontal wells (black lines). (b) Regional location of the ToC2ME program (red box) in Alberta, including both major resource plays in the region the Montney (blue) and Duvernay (red) as well as larger regional context for the location of Alberta in North America (inset). The color version of this figure is available only in the electronic edition.

gradients (Lawson and Hanson, 1974) using an iterative linear least-squares inversion (Paige and Saunders, 1982). The iterative least-squares approach requires a damping parameter. The optimal damping parameter value depends on the relocation method and can be estimated using the L-curve criterion (Fig. S2, available in the supplemental material to this article; Hansen, 2001; Aster *et al.*, 2018). We required a minimum of 10 catalog and 10 cross-correlation observations per pair, limiting pairs to those that shared a significant amount of data. All events are relocated simultaneously. We ran two sets of relocation iterations. Data weights were consistent across relocation iterations with cross-correlation data weighted fully (1.0) and catalog data weighted at half weight (0.5) due to the high quality and number of cross-correlation data for this problem. The first five relocation iterations removed outlier



data over five standard deviations for cross correlations and over three standard deviations for catalog data. The final three iterations also included a distance cutoff removing data for event pairs with a separation larger than 0.18 km.

For the interpretation and analysis of the relocated catalogs, we cluster events using the DBSCAN software (Ester *et al.*, 1996)—a density-based nearest-neighbor clustering tool. The maximum distance between paired points was 20 m, and the minimum sample size to form a cluster of events was three events. Clusters were combined based on proximity using visual inspection. Interpreted faults and fractures were found using a least-squares fit for 3D points based on identified clusters. Strikes and dips were calculated using these planar fits.

Data

The ToC2ME monitored an HF completion west of Fox Creek, Alberta (Eaton *et al.*, 2018) over 35 days on a network of 68 10 Hz geophones in 27 m deep boreholes (Fig. 1a). This HF completion targeted the Duvernay Formation (Fig. 1b), an unconventional hydrocarbon reservoir in the Western Canadian Sedimentary Basin (Weir *et al.*, 2018). An event catalog of 3807 earthquakes was obtained by requiring clear P and S arrivals at a minimum of five stations and well-determined origin times necessary for DT calculations. Bootstrap resampling yielded location uncertainty in terms of 95% confidence intervals of ~10 m in the horizontal directions, and depth uncertainties were ~70 m (Eaton *et al.*, 2018). The original travel-time phase arrival catalog includes 216,328 P -wave arrivals and 227,970 S -wave arrivals for the 3807 events at the 68 geophones.

From the original catalog, we compute DT based on two methods: (1) directly from the catalog by taking differences of arrival times for station pairs and event pairs, and (2) by

Figure 2. (a) Initial catalog locations (dots, scaled by moment magnitude) and outlines (black lines) for wells A–D (left to right) with some of the 3C buried geophones (triangles). Previously interpreted features include fractures SW1–5 (blue-dashed lines; Igonin *et al.*, 2021) and NS1–2 (red-dotted lines; Igonin *et al.*, 2021) and a strike-slip fault (gray dotted-dashed line; Weir *et al.*, 2018). The interpreted top of the Beaverhill Lake Group (background color) is located just below the injection zone ranging from 3.470 to 3.515 km in depth (Igonin *et al.*, 2018). (b) The velocity model is based on well logs showing V_p (black) and V_s (gray) and highlighted depths of several layers of interest seen in panel (c) the simplified stratigraphic column for the study region which shows the Wabamun Group (GP; cyan), the Ireton Formation (FM; orange), the Beaverhill Lake Group (green), and the Precambrian Basement (BSMT; red). The color version of this figure is available only in the electronic edition.

computing waveform cross correlations for station and event pairs. These DT data are the basis for event- and double-pair relocations. For consistency across methods, we used similar parameters to build the DT data, including a maximum inter-event pairing distance of 0.2 km and a minimum interstation pairing distance of 2 km. The maximum number of pairing neighbors is limited to 5, with a required 10 common data observations for pairing. The event-pair data include 187,216 and 177,074 P and S catalog DTs for 12,195 event pairs. The average number of common observations for event pairs is 29, and the average interevent separation distance is 30 m. The double pair data include 203,314 P and 161,059 S DTs. The average interevent separation is 30 m, and the average interstation distance is 3.5 km.

For cross-correlation-based DTs, all possible cross correlations are calculated using unfiltered waveforms. Weighting for

these data comes from the normalized cross-correlation coefficients, and only those data with a cross-correlation coefficient above 0.9 are included in the final selection. To improve the precision of these differential times, 10-fold frequency-domain upsampling (Buttkus, 2000) is applied to produce differential time measurements with subsample precision on already high-sampling rate (500 HZ) waveforms. For event-pair relocations, this process resulted in 12.8 million P cross-correlation times and 8.2 million S cross-correlation times. For the double-pair relocations, there are 37.6 million P and 25.2 million S cross correlations.

Catalog locations were obtained with a 1D layered V_p model determined from sonic logs of a nearby well (Fig. 2b). The V_s values were determined using V_p/V_s ratios from reflection correlations of a multicomponent seismic reflection survey (Weir et al., 2018). This 1D model includes 15 homogeneous layers over a homogeneous half-space, which starts at a depth of 3.6 km. We use this velocity model in our study, eliminating the potential of differences due to velocity model choice.

Results

Event- and double-pair relocations

From the original catalog of 3807 events, we obtained event-pair relocations for 3556 events and double-pair relocations for 3740 events. Some events are removed from the catalog due to lack of arrival-time picks, poor pairing or similarity with other events in the catalog, or due to the iterative removal of outlier differential time measurements (Waldhauser and Ellsworth, 2000; Guo and Zhang, 2017).

Figure 3 summarizes the event locations in terms of cross sections for the original catalog and for the event- and double-pair relocations. Broadly, the cross sections for all three catalogs are consistent, but key differences exist, and the double-pair method produces the clearest image of seismicity. Both relocated catalogs significantly contract locations to spatial clusters that are consistent with pre-existing faults. Furthermore, double-pair relocations produce the sharpest clusters of the three catalogs. In particular, double-pair relocations significantly change event depths to more plausible areas within the Ireton Formation and the top of the Beaverhill Lake Group (Fig. 2c), which is consistent with the depth interval expected for induced seismicity triggered via elevated pore pressure (Igonin et al., 2021). Notably, a northward deepening trend of hypocenters that is evident in the starting and event-pair catalogs is absent in the double-pair relocations.

Figure 4 summarizes the results of linear regressions for which planes are fit to individual clusters in the relocation catalogs. Both relocated catalogs show clear clusters where seismicity locations are in close agreement with planar structures. Double-pair relocations contract more onto planes and resolve more distinct clusters than the event-pair relocations. Two main trends are observed: north–south-oriented clusters (blue) and northeast–southwest-oriented clusters (red; Fig. 4). These

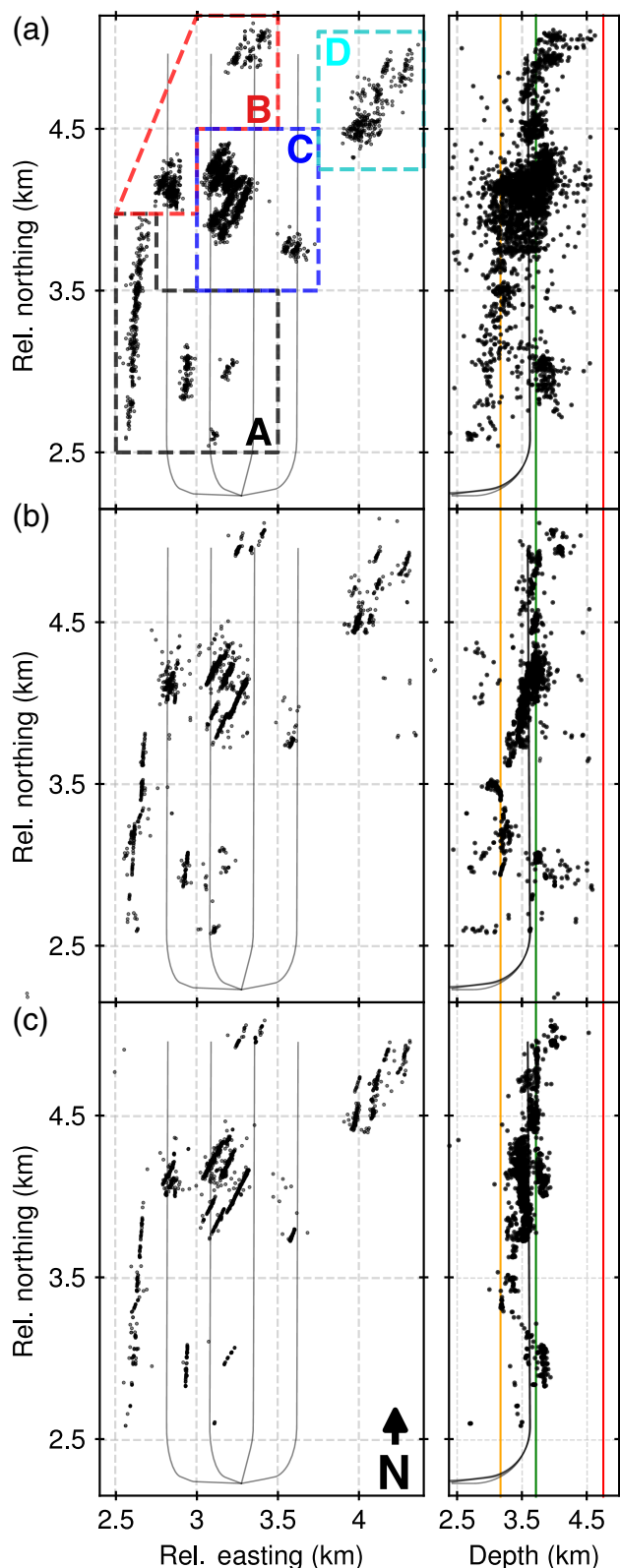


Figure 3. (a) Catalog locations, (b) event-pair relocations, and (c) double-pair relocations for both map view (left) and in-depth (right). Colored lines indicate interfaces for various geologic formations. Injection well outlines (black lines) are also shown. Zones A–D, identified by the dashed polygons, indicate zones of seismicity with similar features. The color version of this figure is available only in the electronic edition.

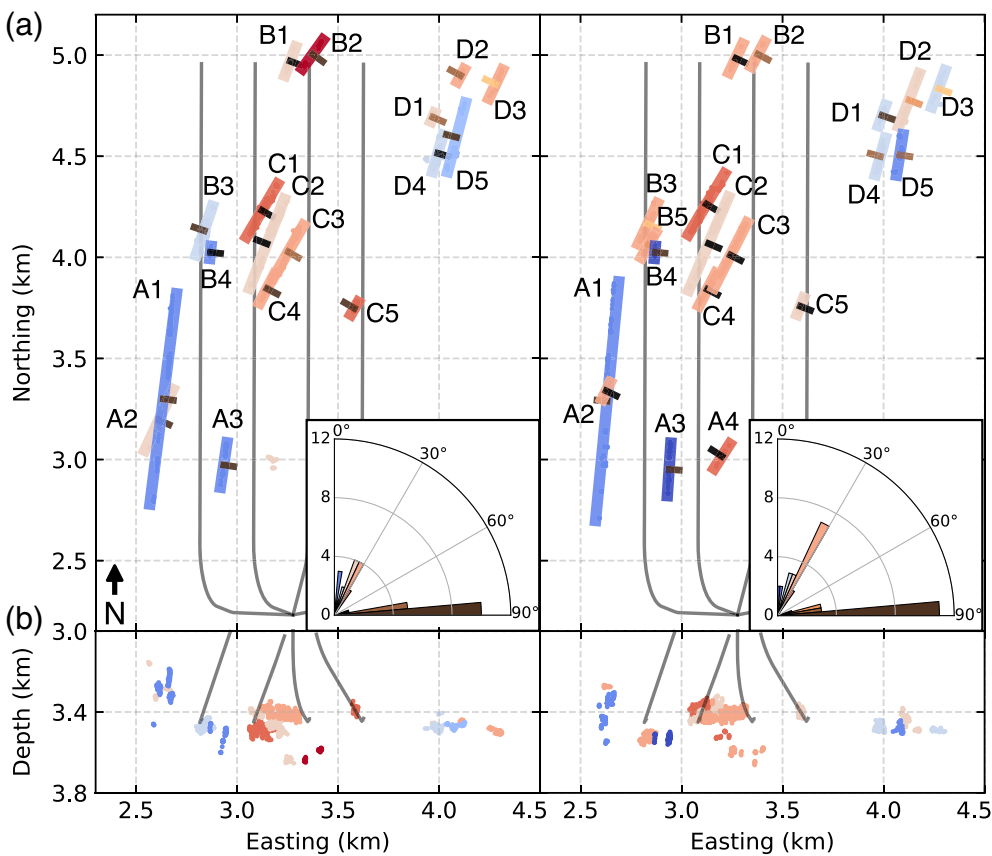


Figure 4. (a) Map view least-squares planar fault fits for geographic event clusters for event-pair (left) and double-pair (right) catalogs. Strikes range from blue (0° – 5°) to red (35° – 40°), and dips range from orange (70° – 75°) to black (85° – 90°). Faults are named based on the seismicity zone from Figure 3a. (b) The east–west projected depth view shows event cluster locations in-depth color-scaled by the cluster’s fault-plane strike. The color version of this figure is available only in the electronic edition.

clusters dip steeply from 70° to 90° with no regional trend. Strikes, dips, and R^2 values (Wright, 1921) from fitting fault planes to these clusters are highlighted in Table S1. Hereafter, we interpret these clusters as faults.

The double-pair relocations improve planar fits and provide more plausible hypocenter depths because the microseismicity is clustered closer to the loci of fluid injection along the HF wells (Fig. 4). The double-pair relocations resolve two additional northeast-southwest-oriented clusters (A4 and B5). In the double-pair catalog, features B3 and B5 appear to form a structural boundary for the northern end of seismicity along cluster A1, where strike-slip motion was triggered (Zhang *et al.*, 2019). The double-pair catalog also provides direct evidence of intersecting faults as inferred by Igonin *et al.* (2021). For example, the northeast-southwest-trending cluster A2 intersects cluster A1. Seismicity along A1 occurs in stages, with seismicity first occurring south of A2 and then migrating from the north end of A1 toward A2 during later treatment stages. Seismicity along A2 occurs after that on A1, indicating that A1 is more favorably oriented within the local stress field and is more critically stressed than fault A2. Possible

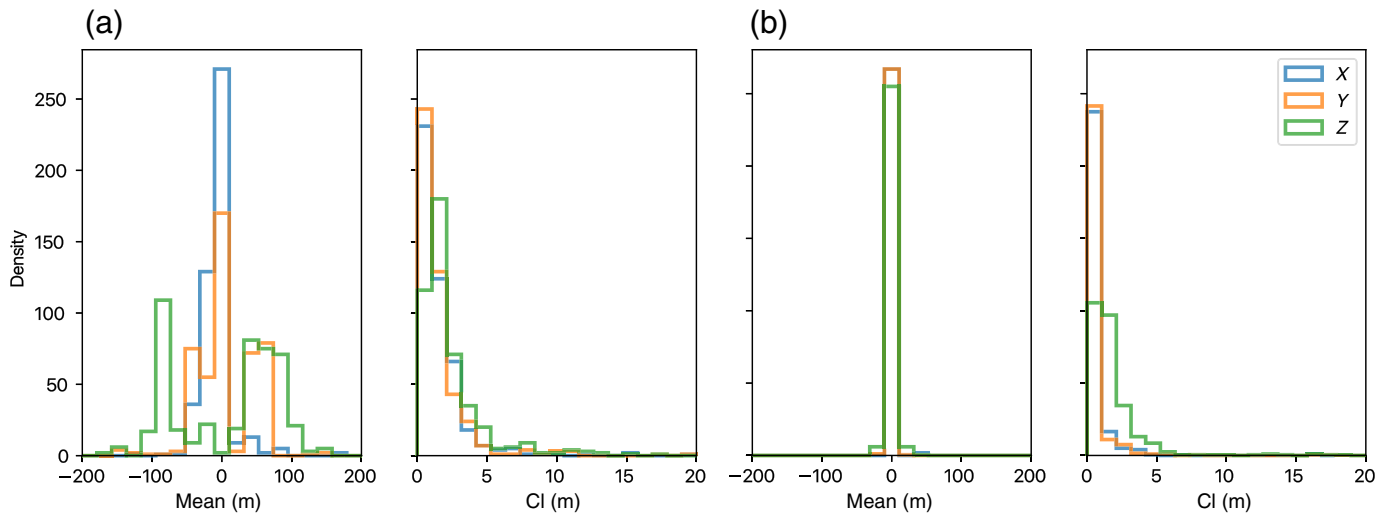
implications for the interpretation of the growth of seismicity over time are considered in the Discussion section.

Relocation uncertainty quantification

To begin, we quantify absolute uncertainty for each catalog using the travel-time residuals for each catalog to estimate absolute uncertainty (Fig. S4). The starting catalog has a mean residual misfit of 0.24 s, meaning that the 1D velocity model used in both the original locations and the relocations is faster than the true velocity structure. The event- and double-pair relocations have the same mean misfit, which remains unchanged after relocation. The width of the 95% confidence interval in travel-time residuals is smaller for both relocation catalogs (−0.004 to 0.783 s for event pair and −0.003 to 0.794 s for double pair) than the starting catalog (−0.042 to 0.791 s). The shifted mean and Gaussian nature of these distributions do indicate

that we remove random location errors from poorly located events or data outliers, but we are left with a catalog bias. In addition, the travel-time residual distributions do vary by zone of seismicity (Fig. S5) with the smallest residuals in Zone A and the narrowest distributions in Zones B and C. Overall, we find that neither relocation catalog improves absolute event locations from the starting catalog.

We quantify relative uncertainty using statistical resampling via bootstrap analysis using the final double-difference residuals as estimates of noise for the relocated hypocenters for the subset of events in Zone A (Billings, 1994; Shearer, 1997; Waldhauser and Ellsworth, 2000). These double-difference residuals are sampled with replacement and added to computed travel times to relocate events. We calculate 250 bootstrap relocation iterations for the subset of events in Zone A, extrapolating these uncertainty estimates as a measure of uncertainty across the data set. Figure 5 shows a comparison of the mean and 95% confidence intervals in X, Y, and Z for the event-and double-pair relocation catalogs. There are notable differences between the two relocation results. The 95% confidence intervals show uncertainties of 2.7, 3.2, and 3.8 m in X, Y, and Z, respectively,



for the event-pair relocations and 1.0, 1.0, and 2.0 in X , Y , and Z , respectively, for the double-pair relocations.

The mean uncertainties (Fig. 5) show notable differences in the event- and double-pair relocations. The double-pair uncertainties are zero mean with a narrow distribution in all three spatial dimensions. The event-pair mean uncertainties exhibit bias (first panel of Fig. 5) in Y and Z with distribution widths in all directions on the order of 10^1 m. Consistent biases in mean uncertainties can result from network geometry, including gaps in station coverage (Michelini and Lomax, 2004). This is not true for the ToC2ME data due to full azimuthal coverage and station symmetry. Furthermore, event-pair relocations reduce sensitivity to path effects near stations. Therefore, biases are likely due to velocity model errors in the source region (Michelini and Lomax, 2004). The double-pair relocations do not show this convergence limitation, likely due to less susceptibility to velocity-model errors in the source region. Anisotropy likely has an impact on the final relocation uncertainties. We interpret the larger event-pair relocation uncertainties and biases in Y and Z as being caused by transverse anisotropy. The 1D velocity model used for relocations (Fig. 2b; Weir *et al.*, 2018) is produced from well logs at a nearby well and does not account for significant lithological variation across the study area, particularly across faults. Possible sources of anisotropy are considered in the *Discussion* section.

Discussion

Methodology strengths and limitations

The work of Guo and Zhang (2017) posits that the double-pair method can improve the absolute locations in depth and improve the relative locations over the event-pair method for data given a sufficient density of both event and station pairs. The high-station density and isotropic station distribution of the ToC2ME data are ideal for studying the limitations of this method. The 68 stations within an area of approximately 7×7 km centered on the injection wells have even azimuthal coverage (Fig. 1). The stations are cemented in shallow boreholes beneath the near-surface layer to increase data quality (Eaton

Figure 5. Relative uncertainty estimates from bootstrapping with individual events for (a) event-pair and (b) double-pair relocations for hypocenters in box A (Fig. 3a) showing both mean uncertainty and 95% confidence intervals (CIs) for all spatial parameters (X , Y , and Z). The color version of this figure is available only in the electronic edition.

et al., 2018). Furthermore, we use 3807 quality-controlled events of sufficient magnitude to produce high-quality arrival-time picks from at least six stations. These events have a high SNR and produce highly correlated waveforms for event and station pairs due to the tight event clustering (e.g., waveforms and waveform cross-correlations in Fig. S1). We automate selecting the regularization parameter using L-curve criteria. Taken together, these conditions are considered ideal for double-pair relocations. The relative locations of the double-pair relocations appear to be improved compared with event-pair relocations and provide a superior image of seismicity. In particular, hypocenter depths are better resolved. However, there is no clear evidence for the improvement of absolute locations.

As illustrated in previous studies, the relative accuracy of event-pair relocations is limited by the accuracy of the velocity model (Michelini and Lomax, 2004). Layered velocity models with sharp contrasts, similar to our velocity model in this case, showed gaps in raytracing and instabilities in final relocation results depending on the event-station separation (Michelini and Lomax, 2004). The ToC2ME velocity model (Fig. 2b) includes sharp velocity contrasts, particularly in the source region. Therefore, we expect limitations due to this velocity model choice.

Both relocation catalogs employ the same velocity model and initial locations, and therefore, both catalogs are limited by the misfit of the interpreted 1D velocity model with the true velocity structure. Double-pair relocations do not improve absolute locations beyond the starting catalog or the event-pair relocations. The consistent 0.24 s travel-time residual for all three catalogs indicates that this value may be the consistent misfit of the

1D velocity model from the true velocity structure. Therefore, catalogs relocated with this velocity model may not be able to improve the absolute location of the catalog beyond this value.

Anisotropy is likely a key reason for the mismatch between the velocity model and the true velocity structure, which impacts relative location uncertainty. Anisotropy is present in the study region due to lithological variations and fracture networks (Weir *et al.*, 2018; Igonin *et al.*, 2022). Both vertical transverse isotropy (VTI) due to depositional layering and horizontal transverse isotropy (HTI) associated with the directional nature of pre-existing fractures in the region are present. Studies of anisotropy in Fox Creek (Li *et al.*, 2019) have indicated that HTI is predominantly northeast–southwest-oriented and results from the combination of north–south-striking faults (such as NS1 and NS2 in Fig. 2a) and northeast–southwest-oriented fractures (such as SW1-5 in Fig. 2a). This HTI shows spatiotemporal changes with seismic activity (Li *et al.*, 2019; Igonin *et al.*, 2022). The uncertainties and biases of event-pair relocations in the Y and Z directions indicate that directional effects and anisotropy are likely the cause.

Based on the relative uncertainties in Y and Z (Fig. 5), both HTI and VTI affect the event-pair relocations because event-pair geometry reduces the impact of path effects in the shallow near-surface zones. Double-pair relocation also reduces source-region path effects that are also diminished, which is the area where anisotropy effects are likely to occur. Anisotropy in the volume occurs at depth in the highly fractured layers with sharp velocity contrasts near the reservoir zone. For this reason, anisotropy has less impact on the double-pair relocations, which show consistently smaller relative uncertainties (Fig. 5). As mentioned in the Theory and Methods section, some of the improvements in the double-pair relocations over the event-pair relocations are likely due to the removal of the origin time correction term as these are now accounted for in changes to the spatial parameters.

Hypocenter depths

The lack of plausible depth estimates in event-pair relocations is likely due to anisotropy (discussed earlier) and sharp velocity contrasts in the 1D velocity model (Michelini and Lomax, 2004). The sharp velocity contrasts in this velocity model led to significant depth stratification in earlier work (Eaton *et al.*, 2018; Zhang *et al.*, 2022). Depth stratification in the initial catalog was the motivation to develop the focal-time analysis method (Poulin *et al.*, 2019), which collocates events based on data from near-surface seismic observations with the 3D reflection-seismic data. This method located events in a distribution centered slightly above the injection depth of 3450 m and is most consistent with the starting locations in this catalog.

Depth estimates from double-pair relocations appear more consistent with prior interpretations of geologic formations and seismicity triggered by changes in pore pressure in these formations. Hence, they are likely less affected by velocity errors along the entire ray path, particularly in the source region, as

previously suggested (Guo and Zhang, 2017). Previous studies have shown that ToC2ME seismicity was triggered by dynamic changes in pore pressure rather than near-field changes in stress. Fluid was injected into the wells, and seismicity was delayed based on the time needed for elevated pore pressure to travel from the injection wells along the permeable corridors (clusters striking at N30°; Igonin *et al.*, 2021). Although there is a significant distance for the pore pressure front to travel in X and Y, the seismicity occurs in a narrow depth interval (Fig. 6).

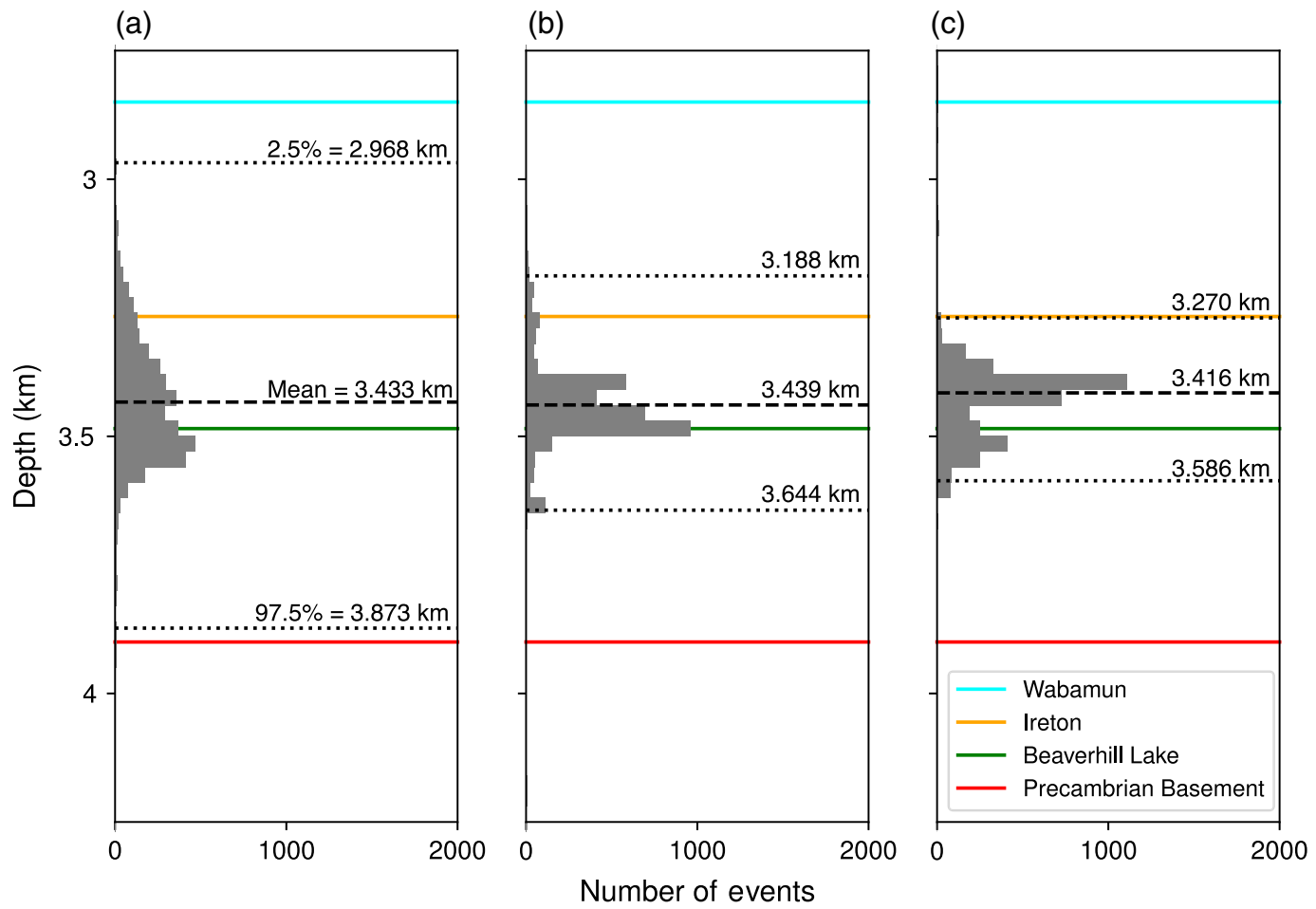
Double-pair relocations provide the most geologically consistent depth intervals of all three catalogs, allowing for a specific interpretation of seismicity behavior in depth. Based on the 95% confidence interval, the starting catalog's depth interval extends over 905 m from the Wabamun to the top of the Precambrian Basement. This depth extent is inconsistent with the analysis of the 3D reflection-seismic data where basement-rooted faults arrest in the Ireton Formation (Eaton *et al.*, 1999; Weir *et al.*, 2018). The depth interval for event-pair relocations is 456 m thick, extending from the lower Wabamun to the upper Beaverhill Lake Formation. For double-pair relocations, the depth interval is 316 m thick, from the top of the Ireton Formation (3.270 km) to the upper Beaverhill Lake (3.586 km). Depths of individual clusters are even more confined, with seismicity of 14 of the 19 identified clusters occurring in narrow depth intervals that are <100 m thick. Preferential permeable fluid migration pathways exist along weaker layers of the interbedded Ireton, Duvernay, and Beaverhill Lake (Swan Hills) Formations. Fluid migration is occurring predominately laterally but is limited in depth.

Only one cluster (A1 in Fig. 4) is activated over the entire depth interval. Significant seismicity occurred along this fault, including one event of moment magnitude 3.2. The presence of feature A2 indicates that permeable pathways allowed for fluid migration from the injection wells to the large fault A1 (Igonin *et al.*, 2021). However, the larger activated depth interval, significant seismicity, and activity in stages (stage 1 activity south of A2 and stage 2 activity north of A2) indicate Coulomb stress transfer may be responsible for the secondary stage of seismicity on A1 (Zhang *et al.*, 2022).

However, systematic location errors exist in the starting catalog and still exist in the relocated catalogs. The mean positive bias in absolute travel-time residuals indicates that the velocity model used in location and relocation is faster than the true velocity structure and, therefore, events may occur at a systematically deeper interval in all relocated catalogs. The relocation of all catalogs (Fig. 6, Fig. S3) to a similar geologically consistent depth interval leads to the conclusion that these locations are robust.

Fault model and interpretation

Our interpretation is consistent with previous work that interpreted the region based on 3D reflection-seismic data as part of a shear zone that is part of a basement-rooted flower structure (Eaton *et al.*,



2018; Igonin *et al.*, 2021; Weir *et al.*, 2022), but we can provide additional constraints on fault orientations, depth intervals for minor faults within the shear corridor, and at which depths faults are activated. These faults are not large enough and do not have enough accumulated slip to appear on seismic surveys.

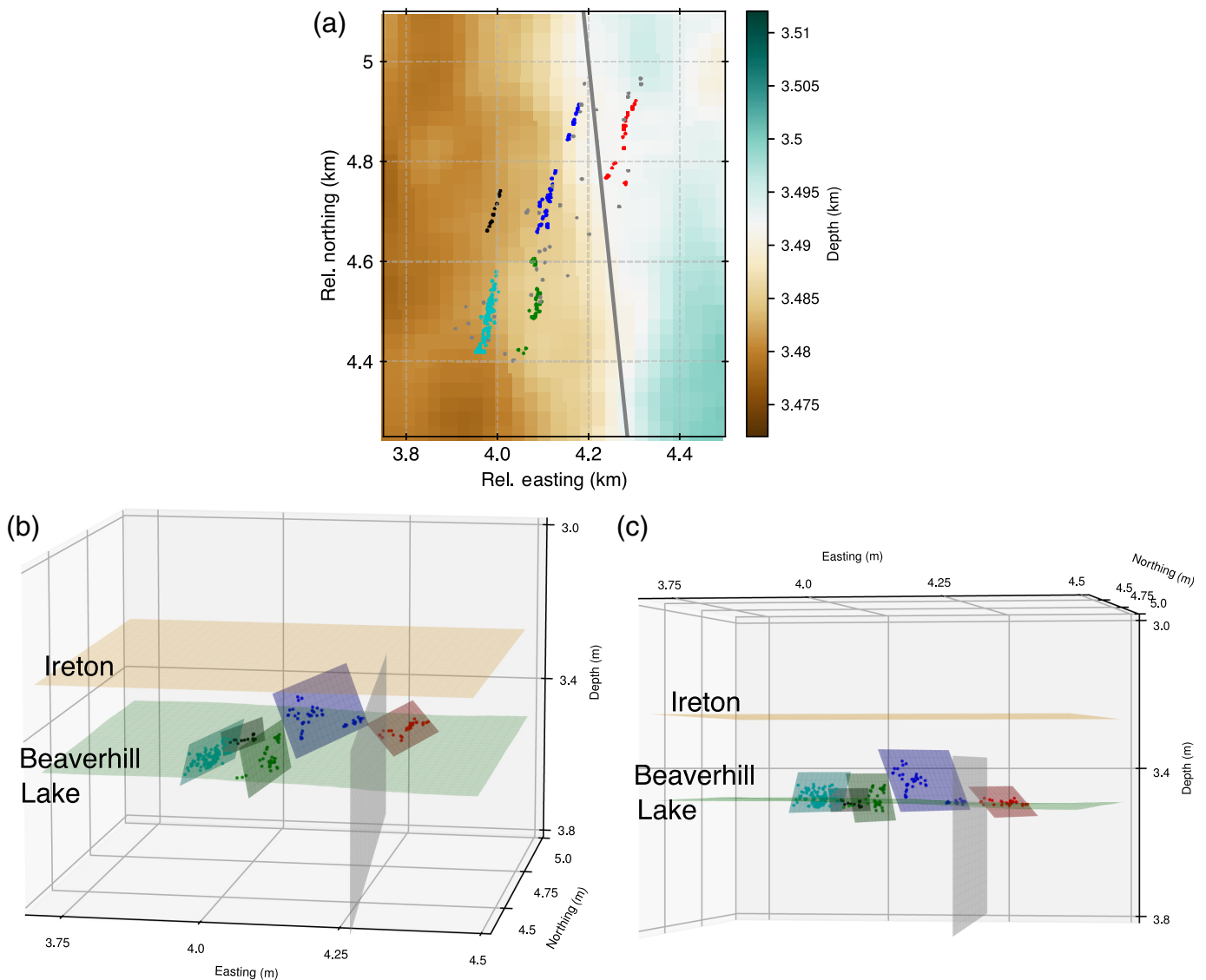
The interpretation of the original catalog (Igonin *et al.*, 2021) shows two right-lateral strike-slip faults with strikes of 5° (NS1 and NS2 in Fig. 2a), and five fracture corridors with 30° strike (SW1-5 in Fig. 2a). Previous work interpreted elevated pore pressure from injection to have traveled along the SW1-5 fracture corridors, activating faults NS1 and NS2 in stages corresponding to the intersections of the northeast-southwest and north-south faults (Igonin *et al.*, 2021). Analysis of 3D seismic data of the study area revealed a large basement-rooted left-lateral strike-slip fault (gray-dotted-dashed line in Fig. 2a) close to the northeast extent of the HF target with 1 km of suspected lateral offset (Weir *et al.*, 2018). The vertical extent of this fault can be traced from the Precambrian Basement through several formations, such as the Beaverhill Lake Formation, and into, but not through, the Ireton Formation (Fig. 2c).

Interpretation of the double-pair relocations (Fig. 4) shows two main structural trends: north-south-trending features (blue lines) and northeast-southwest-trending features (red lines). The two structural trends are oblique to SH_{max} , which

Figure 6. Histograms of hypocenter depths for (a) catalog, (b) event-pair relocations, and (c) double-pair relocations annotated with the 2.5% depth, mean depth, and 97.5% depth intervals for each catalog and notable depth intervals color-coded to match the stratigraphic column (Fig. 2d). The color version of this figure is available only in the electronic edition.

varies from 44° to 64° (Zhang *et al.*, 2019). These trends have been interpreted as Riedel shears (Riedel, 1929) in a bounded shear corridor (Igonin *et al.*, 2021; Weir *et al.*, 2022). The strike-slip fault running through the seismicity in Zone D is the Eastern Boundary fault of the shear corridor (Weir *et al.*, 2022).

The larger north-south clusters, such as A1, A3, and B4, are consistent with strike-slip faults within the structural corridor, showing the existence of many similar faults throughout the corridor. These faults are more optimally oriented for failure in the regional stress state (Zhang *et al.*, 2019), and are larger and more defined than the $N30^\circ$ striking faults. Both fault types, which account for most clusters in the relocated catalog, are Riedel shears, which likely developed during the formation of the fault complex (Weir *et al.*, 2022) and their activated depth intervals over the lower Ireton and upper Beaverhill Lake Formation are consistent with this regional fault's



syndepositional formation with the Ireton Formation. Because these faults form connections between bounding strike-slip faults, a level of asymmetry in both the distribution and pattern of faults is expected (Naylor *et al.*, 1986). Ranges of $\pm 10^\circ$ for both strike and dip (Table S1) are consistent with this range and are the result of differences in when the faults form during the shear corridor formation and where these faults divert from other shears or splay faults (Naylor *et al.*, 1986).

The previously identified fault in the northeast cluster (Fig. 2a) may be of concern for seismic hazard due to a significant amount of left-lateral offset (>1 km) and minor dip-slip offset that occurred in the geological past (Weir *et al.*, 2018). Regional stress indicates that the left-lateral strike-slip fault (striking at $\sim 350^\circ$) is clamped in the current stress regime (Zhang *et al.*, 2019; Weir *et al.*, 2022). The fault extends from the Precambrian basement through most of the Ireton Formation, with deformation likely occurring postdeposition of the Duvernay and is suspected to be permeable (Bao and Eaton, 2016; Weir *et al.*, 2018). Seismicity in Zone D includes several events with magnitudes

Figure 7. Northeast cluster (Zone D) showing (a) map view with shear corridor boundary fault (gray; Weir *et al.*, 2018) with five relocation clusters with background coloring showing depth to Beaverhill Lake Formation. Gray dots show nonclustered double-pair relocations. Panels (b) and (c) show different 3D views of the strike-slip fault (gray) with variously interpreted clusters and fault planes (colored dots and planes). The two horizontal layers are the top of the Ireton (orange) and Beaverhill Lake (green) Formations. The color version of this figure is available only in the electronic edition.

larger than one. Source focal mechanisms for the events in the ToC2ME catalog in this region indicate either right-lateral strike-slip with a northeast–southwest axis or right-lateral oblique dip-slip (Zhang *et al.*, 2019).

From relocated seismicity, we interpret that HF activated the damage zone surrounding the previously identified regional fault (Fig. 7). Relocations show clusters D1, D2, D4, and D5 as oblique features to the west of the fault, whereas cluster

D3 is on the eastern side. Because of lateral offset and sharp lithological variations across the fault, there are poor R^2 fits (Table S1) and large travel-time residuals (Fig. S5) for seismicity in the northeast Zone D clusters. Even though the damage zone is activated and fluid is transferred along the fault's damage zone, there is no evidence of activation of the fault core. Reactivation of this fault as a left-lateral strike-slip fault would be unlikely, given the current regional stress. Features in Zone D show both strike trends associated with Riedel shears forming primary oblique splays ($N5^\circ$) and secondary splays ($N30^\circ$). These splays likely formed during displacement along the larger fault. Clustered seismicity comes within meters of the fault, limiting the immediate damage zone of the strike-slip fault to a narrow zone that is, at most, tens of meters wide (Weir et al., 2018).

Event depths for Zone D are in a narrow depth interval at or above the Ireton–Beaverhill Lake interface in the region of the Duvernay Formation. Although the regional strike-slip fault extends into the Precambrian basement, seismicity does not extend more than 50–100 m into the Beaverhill Lake Formation, which indicates either that the splay faults are discontinuous in depth, there are rheological or geomechanical boundaries limiting pore pressure diffusion and seismicity, or that the fault itself does not conduct fluid past this relatively narrow depth interval. The depths of events in Zone D are consistent with other zones in the catalog, particularly Zone C and clusters B3 and B4. This consistent depth interval across similar features indicates these faults may not extend past this depth interval into the Precambrian basement. Even faults at a deeper interval, such as B1 and B2, are still several hundred meters above the Precambrian basement interface.

Conclusions

We study relocation methods by applying event- and double-pair relocations to the ToC2ME data, with a catalog of 3807 induced earthquakes. The seismicity occurred across a complex fracture and fault system. Double-pair relocations produce sharper images of seismicity where clusters align closely with the interpretation of fault planes. Relative location uncertainties are 1–2 m in all three axis directions and appear to reduce the impact of source-region path effects on locations. Furthermore, hypocenter depths are constrained to a depth region only 316 m thick and show seismicity confined to only two geological units.

From these relocations, we find 19 distinct clusters of events that can be interpreted as seismicity occurring on near-vertical faults trending in two directions: north–south (strikes 0° – 10°) and northeast–southwest (strikes 20° – 35°), which represent two types of critically stressed faults within a regional shear zone. The increased relocation precision, particularly in-depth, indicates that these faults were activated within a narrow depth interval close to the HF depth. Therefore, seismicity occurs in the Ireton and Duvernay Formations and at the top of the

Beaverhill Lake Group but did not migrate in depth as it moved outward from the HF wells. Finally, we image several features in a cluster to the northeast of the HF treatment (Zone D), where seismicity intersects with a regional strike-slip fault. Clusters show activation of Riedel shears on both the west and east sides of the fault but are confined to only the Ireton Formation and the Beaverhill Lake Group. Clearly, changes in pore pressure migrated across the fault, but we see no evidence of seismicity or fluid migration occurring along the fault below 3586 m. Instead, it appears that the pore pressure front propagates along preferential pathways in two geologic units, likely fracture zones or weak lithological layers, spreading on an approximately cylindrical pore pressure front.

Data and Resources

The event catalog used in the article was published in Eaton et al. (2018) and can be found on the associated project GitHub at <https://github.com/ToC2ME> (last accessed December 2021). As event origin times are required to calculate differential times used in double-difference relocation, a further subset of this published catalog included 3807 events with defined origin times. Raw waveform data are available through the Incorporated Research Institutions for Seismology (IRIS) data center using the network code 5B found at <http://ds.iris.edu/mda/5B/?starttime=2016-01-01T00:00:00&endtime=2017-12-31T23:59:59> (last accessed November 2024). The relocation code used in this article is called relocDD-py version 1.0 and can be found on the associated project GitHub (<https://github.com/katie-biegel/relocDD-py>, last accessed October 2024; Biegel and Dettmer, 2024). The supplemental material includes tables and figures not included in the main body of the article, along with files that contain both the event-pair and double-pair relocated catalogs.

Declaration of Competing Interests

The authors acknowledge that there are no conflicts of interest recorded.

Acknowledgments

Research funding for this study came from Alberta Innovates through a Graduate Student Fellowship awarded to K. Biegel. Additional funding came from the Society of Exploration Geophysicists through scholarships awarded to K. Biegel. This research was also funded by a National Science and Engineering Research Council (NSERC) of Canada Discovery Grant to J. Dettmer.

References

- Aster, R. C., B. Borchers, and C. H. Thurber (2018). *Parameter Estimation and Inverse Problems*, Elsevier, Cambridge, Massachusetts.
- Bao, X., and D. W. Eaton (2016). Fault activation by hydraulic fracturing in western Canada, *Science* **354**, 1406–1409, doi: [10.1126/science.aag2583](https://doi.org/10.1126/science.aag2583).
- Biegel, K. M., and J. Dettmer (2024). relocDD-py, available at <https://github.com/katie-biegel/relocDD-py> (last accessed October 2024).
- Billings, S. D. (1994). Simulated annealing for earthquake location, *Geophys. J. Int.* **118**, no. 3, 680–692, doi: [10.1111/j.1365-246X.1994.tb03993.x](https://doi.org/10.1111/j.1365-246X.1994.tb03993.x).

- Buttkus, B. (2000). *Spectral Analysis and Filter Theory in Applied Geophysics*, Springer Science & Business Media, Berlin Heidelberg, Germany.
- Castellanos, F., and M. Van der Baan (2013). Microseismic event locations using the double-difference algorithm, *CSEG Recorder* **38**, no. 3, 26–37.
- Chen, Y., H. Zhang, Y. Miao, Y. Zhang, and Q. Liu (2017). Back azimuth constrained double-difference seismic location and tomography for downhole microseismic monitoring, *Phys. Earth Planet. In.* **264**, 35–46, doi: [10.1016/j.pepi.2016.10.003](https://doi.org/10.1016/j.pepi.2016.10.003).
- Dando, B. D. E., B. P. Goertz-Allmann, D. Kühn, N. Langet, A. M. Dichiariante, and V. Oye (2021). Relocating microseismicity from downhole monitoring of the decatur ccs site using a modified double-difference algorithm, *Geophys. J. Int.* **227**, no. 2, 1094–1122, doi: [10.1093/gji/gjab255](https://doi.org/10.1093/gji/gjab255).
- Deichmann, N., and M. Garcia-Fernandez (1992). Rupture geometry from high-precision relative hypocentre locations of microearthquake clusters, *Geophys. J. Int.* **110**, no. 3, 501–517, doi: [10.1111/j.1365-246X.1992.tb02088.x](https://doi.org/10.1111/j.1365-246X.1992.tb02088.x).
- Dodge, D. A., G. C. Beroza, and W. L. Ellsworth (1995). Foreshock sequence of the 1992 Landers, California, earthquake and its implications for earthquake nucleation, *J. Geophys. Res.* **100**, no. B6, 9865–9880, doi: [10.1029/95JB00871](https://doi.org/10.1029/95JB00871).
- Eaton, D. W., N. Igonin, A. Poulin, R. Weir, H. Zhang, S. Pellegrino, and G. Rodriguez (2018). Induced seismicity characterization during hydraulic-fracture monitoring with a shallow-wellbore geophone array and broadband sensors, *Seismol. Res. Lett.* **89**, no. 5, 1641–1651, doi: [10.1785/0220180055](https://doi.org/10.1785/0220180055).
- Eaton, D. W., G. M. Ross, and J. Hope (1999). The rise and fall of a cratonic arch: A regional seismic perspective on the Peace River Arch, Alberta, *Bull. Can. Petrol. Geol.* **47**, 346–361, doi: [10.35767/gscgbull.47.4.346](https://doi.org/10.35767/gscgbull.47.4.346).
- Ester, M., H. P. Kriegel, J. Sander, and X. Xu (1996). A density-based algorithm for discovering clusters in large spatial databases with noise, *Proc. of the 2nd International Conference on Knowledge Discovery and Data Mining*, Portland, Oregon, AAAI Press, 226–231.
- Fréchet, J. (1985). Sismogenèse et doublets sismiques, *Ph.D. Thesis*, Université Scientifique et Médicale de Grenoble (in French).
- Geiger, L. (1910). Herdbestimmung bei Erdbeben aus den Ankunftszeiten, Nachrichten der K. Gesellschaft der Wissenschaften zu Gottingen, *Math. Phys. Klasse* **1910**, 331–349 (in German).
- Got, J.-L., J. Fréchet, and F. W. Klein (1994). Deep fault plane geometry inferred from multiplet relative relocation beneath the south flank of Kilauea, *J. Geophys. Res.* **99**, no. B8, 15,375–15,386, doi: [10.1029/94JB00577](https://doi.org/10.1029/94JB00577).
- Guo, H., and H. Zhang (2017). Development of double-pair double difference earthquake location algorithm for improving earthquake locations, *Geophys. J. Int.* **208**, 333–348, doi: [10.1093/gji/ggw397](https://doi.org/10.1093/gji/ggw397).
- Guo, H., C. Thurber, I. Warren, B. A. Heath, M. Folsom, H. Sone, N. Lord, J. Akerley, and K. L. Feigl (2023). Enhanced microseismicity during production pumping cessation at the San Emidio geothermal field (Nevada, USA) in December 2016, *J. Geophys. Res.* **128**, no. 11, e2023JB027008, doi: [10.1029/2023JB027008](https://doi.org/10.1029/2023JB027008).
- Hansen, P. C. (2001). The L-curve and its use in the numerical treatment of inverse problems, in *Computational Inverse Problems in Electrocardiography*, P. Johnson (Editor), WIT Press, Southampton, United Kingdom, 119–143.
- Igonin, N., J. P. Verdon, and D. W. Eaton (2022). Seismic anisotropy reveals stress changes around a fault as it is activated by hydraulic fracturing, *Seismol. Res. Lett.* **93**, no. 3, 1737–1752, doi: [10.1785/0220210282](https://doi.org/10.1785/0220210282).
- Igonin, N., J. P. Verdon, J.-M. Kendall, and D. W. Eaton (2021). Large-scale fracture systems are permeable pathways for fault activation during hydraulic fracturing, *J. Geophys. Res.* **126**, no. 3, e2020JB020311, doi: [10.1029/2020JB020311](https://doi.org/10.1029/2020JB020311).
- Igonin, N., M. Zecevic, and D. W. Eaton (2018). Bilinear magnitude-frequency distributions and characteristic earthquakes during hydraulic fracturing, *Geophys. Res. Lett.* **45**, 12,866–12,874, doi: [10.1029/2018GL079746](https://doi.org/10.1029/2018GL079746).
- Ito, A. (1985). High resolution relative hypocenters of similar earthquakes by cross-spectral analysis method, *J. Phys. Earth* **33**, no. 4, 279–294, doi: [10.4294/jpe1952.33.279](https://doi.org/10.4294/jpe1952.33.279).
- Jordan, T. H., and K. A. Sverdrup (1981). Teleseismic location techniques and their application to earthquake clusters in the south-central Pacific, *Bull. Seismol. Soc. Am.* **71**, no. 4, 1105–1130, doi: [10.1785/BSSA0710041105](https://doi.org/10.1785/BSSA0710041105).
- Lawson, C. L., and R. J. Hanson (1974). *Solving Least Squares Problems*, Prentice-Hall, Englewood Cliffs, New Jersey.
- Lees, J. M. (1998). Multiplet analysis at Coso geothermal, *Bull. Seismol. Soc. Am.* **88**, no. 5, 1127–1143, doi: [10.1785/BSSA0880051127](https://doi.org/10.1785/BSSA0880051127).
- Li, C., Z. Peng, D. Yao, H. Guo, Z. Zhan, and H. Zhang (2018). Abundant aftershock sequence of the 2015 7. 5 Hindu Kush intermediate-depth earthquake, *Geophys. J. Int.* **213**, no. 2, 1121–1134, doi: [10.1093/gji/ggy016](https://doi.org/10.1093/gji/ggy016).
- Li, T., Y. J. Gu, Z. Wang, R. Wang, Y. Chen, T.-R. A. Song, and R. Wang (2019). Spatiotemporal variations in crustal seismic anisotropy surrounding induced earthquakes near Fox Creek, Alberta, *Geophys. Res. Lett.* **46**, 5180–5189, doi: [10.1029/2018GL081766](https://doi.org/10.1029/2018GL081766).
- Lomax, A., A. Michelini, and A. Curtis (2014). Earthquake location, direct, global-search methods, in *Encyclopedia of Complexity and Systems Science*, R. Meyers (Editor), Vol. 5, Springer, New York, 2449–2473.
- Lomax, A., J. Virieux, P. Volant, and C. Berge-Thierry (2000). Probabilistic earthquake location in 3D and layered models, in *Advances in Seismic Event Location*, C. H. Thurber and N. Rabinowitz (Editors), Springer, Dordrecht, Netherlands, 101–134.
- Michelini, A., and A. Lomax (2004). The effect of velocity structure errors on double-difference earthquake location, *Geophys. Res. Lett.* **31**, no. 9, L09602, doi: [10.1029/2004GL019682](https://doi.org/10.1029/2004GL019682).
- Naylor, M. A., G. Mandl, and C. H. K. Suppesteijn (1986). Fault geometries in basement-induced wrench faulting under different initial stress states, *J. Struct. Geol.* **8**, 737–752, doi: [10.1016/0191-8141\(86\)90022-2](https://doi.org/10.1016/0191-8141(86)90022-2).
- Ogvari, P. O., H. R. DeShon, and M. J. Hornbach (2018). The Dallas-Fort Worth airport earthquake sequence: Seismicity beyond injection period, *J. Geophys. Res.* **123**, no. 1, 553–563, doi: [10.1002/2017JB015003](https://doi.org/10.1002/2017JB015003).
- Paige, C. C., and M. A. Saunders (1982). LSQR: An algorithm for sparse linear equations and sparse least squares, *ACM Trans. Math. Softw.* **8**, no. 1, 43–71, doi: [10.1145/355984.355989](https://doi.org/10.1145/355984.355989).
- Pavlis, G. L. (1986). Appraising earthquake hypocenter location errors: A complete, practical approach for single-event locations, *Bull. Seismol. Soc. Am.* **76**, no. 6, 1699–1717, doi: [10.1785/BSSA0760061699](https://doi.org/10.1785/BSSA0760061699).

- Pavlis, G. L. (1992). Appraising relative earthquake location errors, *Bull. Seismol. Soc. Am.* **82**, no. 2, 836–859, doi: [10.1785/BSSA0820020836](https://doi.org/10.1785/BSSA0820020836).
- Poulin, A., R. Weir, D. W. Eaton, N. Igonin, Y. Chen, L. Lines, and D. Lawton (2019). Focal-time analysis: A new method for stratigraphic depth control of microseismicity and induced seismic events, *Geophysics* **84**, no. 6, KS173–KS182, doi: [10.1190/geo2019-0046.1](https://doi.org/10.1190/geo2019-0046.1).
- Poupinet, G., W. L. Ellsworth, and J. Frechet (1984). Monitoring velocity variations in the crust using earthquake doublets: An application to the Calaveras Fault, California, *J. Geophys. Res.* **89**, no. B7, 5719–5731, doi: [10.1029/JB089iB07p05719](https://doi.org/10.1029/JB089iB07p05719).
- Riedel, W. (1929). Zur mechanik geologischer brucherscheinungen. zentral-blatt fur mineralogie, *Geol. Paleontol.* **B**, 354–368 (in German).
- Rodi, W. (2006). Grid-search event location with non-Gaussian error models, *Phys. Earth Planet. In.* **158**, no. 1, 55–66, doi: [10.1016/j.pepi.2006.03.010](https://doi.org/10.1016/j.pepi.2006.03.010).
- Sambridge, M. S., and B. L. N. Kennett (2001). Seismic event location: Nonlinear inversion using a neighbourhood algorithm, *Pure Appl. Geophys.* **158**, no. 1, 241–257.
- Schaff, D. P., G. H. R. Bokelmann, G. C. Beroza, F. Waldhauser, and W. L. Ellsworth (2002). High-resolution image of Calaveras fault seismicity, *J. Geophys. Res.* **107**, no. B9, ESE-5, doi: [10.1029/2001JB000633](https://doi.org/10.1029/2001JB000633).
- Scherbaum, F., and J. Wendler (1986). Cross spectral analysis of Swabian Jura (SW Germany) three-component microearthquake recordings, *J. Geophys.* **60**, no. 1, 157–166.
- Share, P.-E., R. R. Castro, J. A. Vidal-Villegas, L. Mendoza, and Y. Ben-Zion (2021). High-resolution seismic imaging of the plate boundary in northern Baja California and southern California using double-pair double-difference tomography, *Earth Planet. Sci. Lett.* **568**, 117004, doi: [10.1016/j.epsl.2021.117004](https://doi.org/10.1016/j.epsl.2021.117004).
- Shearer, P. M. (1997). Improving local earthquake locations using the L1 norm and waveform cross correlation: Application to the Whittier Narrows, California, aftershock sequence, *J. Geophys. Res.* **102**, no. B4, 8269–8283, doi: [10.1029/96JB03228](https://doi.org/10.1029/96JB03228).
- Tian, X., W. Zhang, and J. Zhang (2016). Cross double-difference inversion for microseismic event location using data from a single monitoring well, *Geophysics* **81**, no. 5, KS183–KS194, doi: [10.1190/geo2016-0198.1](https://doi.org/10.1190/geo2016-0198.1).
- VanDecar, J. C., and R. S. Crosson (1990). Determination of teleseismic relative phase arrival times using multi-channel cross-correlation and least squares, *Bull. Seismol. Soc. Am.* **80**, no. 1, 150–169, doi: [10.1785/BSSA0800010150](https://doi.org/10.1785/BSSA0800010150).
- Waldhauser, F., and W. L. Ellsworth (2000). A double-difference earthquake location algorithm: Method and application to the northern Hayward fault, California, *Bull. Seismol. Soc. Am.* **90**, no. 6, 1353–1368, doi: [10.1785/0120000006](https://doi.org/10.1785/0120000006).
- Waldhauser, F., and D. P. Schaff (2008). Large-scale relocation of two decades of Northern California seismicity using cross-correlation and double-difference methods, *J. Geophys. Res.* **113**, no. B8, doi: [10.1029/2007JB005479](https://doi.org/10.1029/2007JB005479).
- Waldhauser, F., W. L. Ellsworth, D. P. Schaff, and A. Cole (2004). Streaks, multiplets, and holes: High-resolution spatio-temporal behavior of Parkfield seismicity, *Geophys. Res. Lett.* **31**, no. 18, L18608, doi: [10.1029/2004GL020649](https://doi.org/10.1029/2004GL020649).
- Weir, R., D. W. Eaton, T. Eyre, and D. C. Lawton (2022). Integrated interpretation: Defining risk corridors by combining 3-D seismic interpretation with induced seismicity hypocenters, *Tectonophysics* **827**, 229263, doi: [10.1016/j.tecto.2022.229263](https://doi.org/10.1016/j.tecto.2022.229263).
- Weir, R., D. W. Eaton, L. R. Lines, D. C. Lawton, and E. Ekpo (2018). Inversion and interpretation of seismic-derived rock properties in the Duvernay play, *Interpretation* **6**, no. 2, SE1–SE14, doi: [10.1190/INT-2017-0149.1](https://doi.org/10.1190/INT-2017-0149.1).
- Wolfe, C. J. (2002). On the mathematics of using difference operators to relocate earthquakes, *Bull. Seismol. Soc. Am.* **92**, no. 8, 2879–2892, doi: [10.1785/0120010189](https://doi.org/10.1785/0120010189).
- Wright, S. (1921). Correlation and causation, *J. Agric. Res.* **20**, 557–585.
- Zhang, F., R. Wang, Y. Chen, and Y. Chen (2022). Spatiotemporal variations in earthquake triggering mechanisms during multistage hydraulic fracturing in western Canada, *J. Geophys. Res.* **127**, e2022JB024744, doi: [10.1029/2022JB024744](https://doi.org/10.1029/2022JB024744).
- Zhang, H., D. W. Eaton, G. Rodriguez, and S. Q. Jia (2019). Source-mechanism analysis and stress inversion for hydraulic-fracturing-induced event sequences near Fox Creek, Alberta, *Bull. Seismol. Soc. Am.* **109**, 636–651, doi: [10.1785/0120180275](https://doi.org/10.1785/0120180275).
- Zhang, H., R. M. Nadeau, and M. N. Toksoz (2010). Locating non-volcanic tremors beneath the San Andreas fault using a station-pair double-difference location method, *Geophys. Res. Lett.* **37**, no. 13, L13304, doi: [10.1029/2010GL043577](https://doi.org/10.1029/2010GL043577).

Manuscript received 10 May 2024

Published online 4 December 2024